The instability of non-Newtonian boundary-layer flows over rough rotating disks

A. A. Alqarni[a], B. Alveroğlu[b], P. T. Griffiths[c], S. J. Garrett[d,*]

[a]*Department of Engineering, University of Leicester, Leicester, LE1 7RH, UK*
[b]*Department of Mathematics, Bursa Technical University, Bursa, 16330, Turkey*
[c]*Department of Mathematics, Coventry University, Coventry, CV1 5FB, UK*
[d]*School of Mathematics & Actuarial Science, University of Leicester, Leicester, LE1 7RH, UK*

Abstract

We are concerned with the local linear convective instability of the incompressible boundary-layer flows over rough rotating disks for non-Newtonian fluids. Using the Carreau model for a range of shear-thinning and shear-thickening fluids, we determine, for the first time, steady-flow profiles under the partial-slip model for surface roughness. The subsequent linear stability analyses of these flows (to disturbances stationary relative to the disk) indicate that isotropic and azimuthally-anisotropic (radial grooves) surface roughness leads to the stabilisation of *both* shear-thinning and -thickening fluids. This is evident in the behaviour of the critical Reynolds number and growth rates of both Type I (inviscid cross flow) and Type II (viscous streamline curvature) modes of instability. The underlying physical mechanisms are clarified using an integral energy equation.

Keywords: Laminar boundary layer, non-Newtonian, Carreau fluid, Convective instability

1. Introduction

The hydrodynamic instability of the rotating-disk system has long been used to investigate the fundamental transition mechanisms of three-dimensional boundary layers. The pioneering study of the steady incompressible flow induced by the rotation of a smooth, infinite plane with a fixed angular velocity was performed by von Kármán [1]. He showed that the flow is an exact solution of the Navier–Stokes equations and is characterised by a negligible centrifugal force close to the disk surface. The centrifugal force and the pressure gradient on the fluid are not balanced and the flow spirals outwards, with mass conservation maintained by a downwards axial flow that entrains fluid into the boundary layer. The resulting velocity distribution in the boundary layer is three-dimensional and has an inflectional profile in the radial direction.

*Corresponding author
Email address: stephen.garrett@le.ac.uk (S. J. Garrett)

Gregory *et al.* [2] investigated the stability of the von Kármán flow and performed experimental and theoretical studies at high Reynolds numbers. This led to the discovery of spiral vortex disturbances within the boundary layer. Later, Malik [3] computed the neutral curves associated with disturbances stationary relative to the disk surface and found two instability modes: one governed by an inviscid crossflow mechanism and the other by viscous streamline-curvature mechanisms. At a similar time, Hall [4] conducted a rigorous asymptotic study of the two stability branches and found complete agreement with Malik's neutral curve in the high Reynolds-number limit. The inviscid and viscous modes have subsequently been designated Type I and Type II modes, respectively.

Two theoretical models exist in the literature for the steady boundary-layer flow over *rough* rotating disks. These were introduced by Miklavčič and Wang [5] and Yoon et al. [6] and are henceforth referred to as the MW and YHP models, respectively. Both models demonstrate how surface roughness could lead to modifications to the classic von Kármán solution over a smooth disk. The two models are, however, fundamentally different in their formulation. The YHP model imposes a surface roughness function on the disk surface along the radial direction and assumes rotational symmetry. This model therefore leads to a particular case of anisotropic roughness composed of concentric grooves; the roughness is felt as one traverses the disk in the radial direction. In contrast, the MW approach models the surface roughness by replacing the usual no-slip conditions at the disk surface with partial-slip conditions. By modifying the boundary conditions in the radial and azimuthal directions, the MW approach can independently model roughness in these two directions. This leads to isotropic roughness when the roughness parameters are identical in both directions, and anisotropic roughness when they differ. Owing to its greater flexibility, the MW approach has received detailed attention for Newtonian fluids and will be used throughout this investigation.

Under the MW formulation, Cooper et al. [7] examined the possibility of delaying the onset of instability within the rotating-disk system via the introduction of distributed surface roughness. Their convective stability analysis considered both isotropic and anisotropic surface roughnesses and led to the clear conclusion that surface roughness stabilises the Type I mode. In contrast, the Type II mode is destabilised significantly by anisotropic roughness in the form of the concentric grooves. Following this, Garrett et al. [8] considered the effects on the stability predictions of using the two roughness models. Similar results were found under the MW and YHP models for the Type I modes, but differences in the response of the Type II mode were observed. In particular, Reynolds-stress energy production increases with the roughness level and the increase is slightly less pronounced for the YHP model than for the MW model.

Complementary research continues using the MW model. For example, Stephen [9] has recently confirmed the neutral curve of Cooper *et al.* using a rigorous asymptotic approach. Furthermore, Alveroglu et al.[10, 11] has extended Cooper *et al.*'s work to the entire BEK family of boundary-layer flows (i.e., Bödewadt, Ekman and von Kármán). Again surface roughness is found to be universally stabilising for the dominant Type I mode. However, increased concentric grooves causes destabilisation of the Type II mode as it moves upstream and eventually becomes the critical mode at the lowest Reynolds number.

Returning to smooth rotating disks, the literature shows a growing interest in the effects of non-Newtonian boundary-layer flows. Fundamental to the modelling of non-Newtonian flows is the underlying viscosity model and a good overview of the most widely used models can be found in Bird et al. [12]. Mitschka [13] was the first to generalise the von Kármán solution to non-Newtonian flows and used a power-law fluid. More recently, the base flows for various generalised Newtonian models have been derived by Griffiths [14]. He then proceeds to explore convective instability characteristics of the models[15, 16], utilising both asymptotic and numerical methods. In particular, the power-law studies are extended to include more sophisticated models due to Bingham [17] and Carreau [18]. Griffiths demonstrates that, unlike the power-law and Bingham models, the Carreau model preserves the von Kármán similarity solution which has mathematical advantages within the formulation. Furthermore, the Carreau model is adopted here due to the limitation of the power-law especially for very low and very high shear rates. In general, linear stability analyses investigated in the rotating disk boundary layer have revealed that different results are reached when power-law shear-thinning results are compared to those owing from the Carreau fluid model [19]. Thereby, the growing interest in the Carreau fluids has been the motivation for the current investigation.

The objective of this investigation is to examine the linear convective instability of the non-Newtonian boundary-layer flow over rough rotating disks. The MW (partial-slip) model for surface roughness and Carreau viscosity model will be used. Section 2 presents the complete mathematical formulation of our study. This includes the steady flow, perturbation equations and derivation of the energy analysis equations. The resulting mean-flow velocity profiles and stability analysis are presented and discussed in §3. Our conclusions are drawn in §4.

2. Mathematical formulation

2.1. Mean flow

We follow the approach developed by Griffiths [14] to obtain the mean-flow flow profiles under the Carreau [18] viscosity model. However, modifications are made to incorporate the

partial-slip approach to surface roughness. The disk is assumed to be of an infinite radius and rotating at a constant angular velocity, Ω^*, within an incompressible Carreau fluid. We work with cylindrical polar co-ordinates within the rotating reference frame and the governing equations are given by

$$\boldsymbol{\nabla \cdot u^*} = 0, \tag{1a}$$

$$\frac{\partial \boldsymbol{u^*}}{\partial t^*} + \boldsymbol{u^* \cdot \nabla u^*} + \boldsymbol{\Omega^* \times (\Omega^* \times r^*)} + 2\boldsymbol{\Omega^* \times u^*} = -\frac{1}{\rho^*}\nabla p^* + \frac{1}{\rho^*}\boldsymbol{\nabla \cdot \tau^*}. \tag{1b}$$

Here $\boldsymbol{u^*} = (U^*, V^*, W^*)$ is the total velocity vector; t^* is time; p^* is the fluid pressure; $\boldsymbol{r^*} = (r^*, 0, z^*)$ is the position vector in space; $\boldsymbol{\Omega^*} = (0, 0, \Omega^*)$ is the constant angular velocity; and ρ^* is the fluid density. An asterisk, where used, refers to dimensional variable.

The stress tensor for generalised Newtonian models is given by $\boldsymbol{\tau^*} = \mu^*\ddot{\boldsymbol{\gamma}}^*$, where $\mu^* = \mu^*(\ddot{\gamma}^*)$ is the non-Newtonian viscosity. The magnitude of the rate of strain tensor is given by $\ddot{\gamma}^* = \sqrt{(\ddot{\boldsymbol{\gamma}}^* : \ddot{\boldsymbol{\gamma}}^*)/2}$ and, for a Carreau fluid, we have

$$\mu^*(\ddot{\gamma}^*) = \mu^*_\infty + (\mu^*_0 - \mu^*_\infty)\left[1 + (\lambda^*\ddot{\gamma}^*)^2\right]^{(n-1)/2}. \tag{2}$$

Here the power index n characterises the fluid behaviour such that it is *shear-thinning* when $n < 1$, Newtonian when $n = 1$ and *shear-thickening* when $n > 1$. The quantities μ^*_0 and μ^*_∞ denote the zero-shear-rate and infinite-shear-rate viscosities, respectively, and λ^* is referred to as the time constant or 'relaxation time'. In practical applications, the zero-shear-rate viscosity is typically three to four orders of magnitude larger than the infinite-shear-rate viscosity and, in view of this, μ^*_∞ is neglected in the current analysis.

Under the boundary-layer approximation, Eq. 1 is expressed at leading order as

$$\frac{1}{r^*}\frac{\partial (r^* U^*_0)}{\partial r^*} + \frac{1}{r^*}\frac{\partial V^*_0}{\partial \theta} + \frac{\partial W^*_0}{\partial z^*} = 0, \tag{3a}$$

$$\frac{\partial U^*_0}{\partial t^*} + U^*_0\frac{\partial U^*_0}{\partial r^*} + \frac{V^*_0}{r^*}\frac{\partial U^*_0}{\partial \theta} + W^*_0\frac{\partial U^*_0}{\partial z^*} - \frac{(V^*_0 + r^*\Omega^*)^2}{r^*} = \frac{1}{\rho^*}\frac{\partial P^*_0}{\partial r^*} + \frac{1}{\rho^*}\frac{\partial}{\partial z^*}\left(\mu\frac{\partial U^*_0}{\partial z^*}\right), \tag{3b}$$

$$\frac{\partial V^*_0}{\partial t^*} + U^*_0\frac{\partial V^*_0}{\partial r^*} + \frac{V^*_0}{r^*}\frac{\partial V^*_0}{\partial \theta} + W^*_0\frac{\partial V^*_0}{\partial z^*} + \frac{U^*_0 V^*_0}{r^*} + 2\Omega^* U^* = \frac{1}{\rho^* r^*}\frac{\partial P^*_0}{\partial \theta^*} + \frac{1}{\rho^*}\frac{\partial}{\partial z^*}\left(\mu\frac{\partial V^*_0}{\partial z^*}\right), \tag{3c}$$

$$\begin{aligned}\frac{\partial W^*_0}{\partial t^*} + U^*_0\frac{\partial W^*_0}{\partial r^*} + \frac{V^*_0}{r^*}\frac{\partial W^*_0}{\partial \theta} + W^*_0\frac{\partial W^*_0}{\partial z^*} = &-\frac{1}{\rho^*}\frac{\partial P^*_1}{\partial z^*} \\ &+ \frac{1}{\rho^* r^*}\frac{\partial}{\partial r^*}\left(\mu r^*\frac{\partial U^*_0}{\partial z^*}\right) + \frac{1}{\rho^* r^*}\frac{\partial}{\partial \theta}\left(\mu\frac{\partial V^*_0}{\partial z^*}\right) + \frac{2}{\rho^*}\frac{\partial}{\partial z^*}\left(\mu\frac{\partial W^*_0}{\partial z^*}\right),\end{aligned} \tag{3d}$$

where (U_0^*, V_0^*, W_0^*) are the leading-order velocities, (P_0^*, P_1^*) are the pressure components and the viscosity function μ^* is given by

$$\mu = \mu_0^* \left\{ 1 + (\lambda^*)^2 \left[\left(\frac{\partial U_0^*}{\partial z^*} \right)^2 + \left(\frac{\partial V_0^*}{\partial z^*} \right)^2 \right] \right\}^{(n-1)/2}. \tag{4}$$

Following Griffiths [20], Eq. 4 can be normalised with respect to μ_0^* in order to facilitate direct quantitative comparisons with the corresponding Newtonian mean-flow profiles.

The dimensionless steady and axisymmetric mean-flow components are scaled as

$$U(z) = \frac{U_0^*}{r^*\Omega^*}, \quad V(z) = \frac{V_0^*}{r^*\Omega^*}, \quad W(z) = \frac{W_0^*}{l^*\Omega^*}, \quad P(z) = \frac{P_1^*}{\rho^* {l^*}^2 {\Omega^*}^2},$$

where $l^* = \left[\frac{\nu^*}{\Omega^*}\right]^{(1/2)}$ is a characteristic length scale. These lead to the following non-dimensional equations for the mean flow

$$2U + W' = 0, \tag{5a}$$

$$U^2 - (V+1)^2 + WU' - (\mu U')' = 0, \tag{5b}$$

$$2U\,(V+1) + WV' - (\mu V')' = 0, \tag{5c}$$

$$WW' + P' - qU' + 2\mu' U - (\mu W')' = 0. \tag{5d}$$

where a prime denotes a derivative with respect to z and

$$q = \frac{k^2(n-1)\mu[(U')^2 + (V')^2]}{1 + k^2[(U')^2 + (V')^2]}, \quad \mu = \left\{ 1 + k^2[(U')^2 + (V')^2] \right\}^{(n-1)/2}, \quad k = r^*\lambda^*\Omega^*(\nu/\Omega)^{-1/2}.$$

Note that under the Carreau model, viscosity is a function of r which technically prohibits such a similarly-type solution. However, we proceed to conduct local stability analyses at fixed positions and, in practice, the variable r will take particular fixed values. The use of the similarity solution is therefore permitted as an approximation; this approach was also used in Griffiths [20].

We now proceed to use the MW model [5] for surface roughness to determine the boundary conditions at the disk surface. This approach assumes that roughness can be modelled using partial-slip conditions instead of the usual no-slip conditions at the disk surface, whereas the boundary condition at the upper edge of the boundary layer is identical to the smooth-disk formulation. To derive the boundary conditions we adopt the method proposed by Navier [21], from which the partial-slip condition in the radial and azimuthal directions are respectively given by

$$U\,|_{z=0} = \lambda \tau_r^z\,|_{z=0}, \quad V\,|_{z=0} = \eta \tau_\theta^z\,|_{z=0}\,.$$

Here λ and η are the respective the slip coefficients defined as,

$$\lambda = \lambda_1 \mu \sqrt{\frac{\Omega^* l^{*2}}{\nu^*}} \quad \text{and} \quad \eta = \eta_1 \mu \sqrt{\frac{\Omega^* l^{*2}}{\nu^*}}. \tag{6}$$

where $\nu^* = \left[\frac{\mu_o^*}{\rho^*}\right]$. Using the above transformations, Eq. 6 enables the boundary conditions to be determined as

$$\left.\begin{aligned} U &= \lambda\, U'[1 + k^2(U'^2 + V'^2)]^{(n-1)/2} \\ V &= \eta\, V'[1 + k^2(U'^2 + V'^2)]^{(n-1)/2} \\ W &= 0 \end{aligned}\right\} \text{at} z = 0, \tag{7}$$

and

$$U = 0,\ V = -1 \quad \text{as}\, z \to \infty. \tag{8}$$

The coefficients λ and η give a measure of the roughness in the radial and azimuthal directions, respectively. When $\lambda = \eta = 0$ the boundary conditions reduce to the no-slip boundary conditions for a smooth disk. The scenario of anisotropic roughness is exemplified by concentric grooves ($\eta > 0, \lambda = 0$) and radial grooves ($\eta = 0, \lambda > 0$); whereas isotropic roughness corresponds to the case $\lambda = \eta > 0$.

In the particular case that $n = 1$ and $\lambda = \eta = 0$, the system defined by Eqs. (5), (7) and (8) reduces to the standard von Kármán system. Similarly, when $n = 1$ and $\lambda \neq 0$, $\eta \neq 0$ we recover the governing equations for the standard MW model [5] for Newtonian fluids.

2.2. Convective instability

A local linear instability analysis will be conducted on the steady mean-flow system. As discussed in [7, 10], the partial-slip boundary conditions do not affect the perturbation equations; that is, the governing stability equations are unaffected by surface roughness within the MW model. However, the perturbation equations are affected by the underlying viscosity model and we present their detailed derivation here. The system of Eq. 3 is used here to derive the perturbations equations for the Carreau fluid. Perturbations are applied at a specific radius by imposing sufficiently small disturbances on the steady-mean flow at some fixed local Reynolds number, defined as

$$Re = \frac{\Omega^* r_a^* l^*}{\nu^*} = r_a. \tag{9}$$

The velocity, pressure and time are cast in dimensionless form using the scalings $r_a^*\Omega^*$, $\rho^*(r_a^*\Omega^*)$ and $l^*/(r_a^*\Omega^*)$, respectively. The instantaneous non-dimensional velocities and pressure component including the mean values and small perturbations are therefore given by

$$U_0(r, \theta, z, t) = \frac{r}{Re} U(z) + u(r, \theta, z, t), \tag{10a}$$

$$V_0(r,\theta,z,t) = \frac{r}{Re}V(z) + v(r,\theta,z,t), \tag{10b}$$

$$W_0(r,\theta,z,t) = \frac{1}{Re}W(z) + w(r,\theta,z,t), \tag{10c}$$

$$P_{0,1}(r,\theta,z,t) = \frac{1}{Re^2}P(z) + p(r,\theta,z,t), \tag{10d}$$

where u,v, w and p are small perturbation quantities. At this stage it is necessary to apply the so called *parallel-flow approximation* to ensure the linearised equations are separable in r, θ and t. This involves replacing the variable r with the local Reynolds number and neglecting all terms $\mathcal{O}(Re^{-2})$, leading to

$$\frac{u}{Re} + \frac{\partial u}{\partial r} + \frac{1}{Re}\frac{\partial v}{\partial \theta} + \frac{\partial w}{\partial z} = 0, \tag{11a}$$

$$\Delta_1 u + U'w + \frac{Uu - 2(V+1)v}{Re} = -\frac{\partial p}{\partial r} + \frac{1}{Re}\left[\mu\Delta_2 u + \mu'\left(\frac{\partial u}{\partial z} + \frac{\partial w}{\partial r}\right) + \frac{\partial(\tilde{\mu}U'\psi)}{\partial z}\right], \tag{11b}$$

$$\Delta_1 v + V'w + \frac{Uv + 2(V+1)u}{Re} = -\frac{1}{Re}\frac{\partial p}{\partial \theta} + \frac{1}{Re}\left[\mu\Delta_2 v + \mu'\left(\frac{\partial v}{\partial z} + \frac{1}{Re}\frac{\partial w}{\partial \theta}\right) + \frac{\partial(\tilde{\mu}V'\psi)}{\partial z}\right], \tag{11c}$$

$$\Delta_1 w + \frac{W'w}{Re} = -\frac{\partial p}{\partial z} + \frac{1}{Re}\left[\mu\Delta_2 w + 2\mu'\frac{\partial w}{\partial z} + \tilde{\mu}\left(U'\frac{\partial}{\partial r} + \frac{V'}{Re}\frac{\partial}{\partial \theta}\right)\psi\right], \tag{11d}$$

where

$$\Delta_1 = \frac{\partial}{\partial t} + U\frac{\partial}{\partial r} + \frac{V}{Re}\frac{\partial}{\partial \theta} + \frac{W}{Re}\frac{\partial}{\partial z},$$
$$\Delta_2 = \frac{\partial^2}{\partial r^2} + \frac{1}{Re^2}\frac{\partial^2}{\partial \theta^2} + \frac{\partial^2}{\partial z^2},$$
$$\tilde{\mu} = \frac{k^2(n-1)\mu}{1 + k^2[(U')^2 + (V')^2]},$$
$$\psi = \left(U'\frac{\partial u}{\partial z} + V'\frac{\partial v}{\partial z}\right).$$

In Eq. 11, the terms containing ψ are associated with the perturbation of viscosity induced by the velocity perturbations.

We then proceed by assuming the normal-mode form for the perturbing quantities

$$(u, v, w, p) = (\hat{u}, \hat{v}, \hat{w}, \hat{p})(z; \alpha, \beta, \omega; Re, k)e^{\mathrm{i}(\alpha r + \beta\theta - \omega t)}.$$

Here $\alpha = \alpha_\mathrm{r} + \mathrm{i}\alpha_\mathrm{i}$ is the radial wave number, β is the azimuthal wave number (which is real) and ω is the frequency of the disturbances expressed in the rotating frame. We therefore rewrite Eq. 11 in the form of a nonlinear eigenvalue problem as

$$\alpha(\mathrm{i}\hat{u}) + \left(\frac{\hat{u}}{Re} + \mathrm{i}\beta\hat{v} + \hat{w}'\right) = 0, \tag{12a}$$

$$\alpha^2\left(\frac{\mu\hat{u}}{Re}\right)+\alpha\left[\mathrm{i}\left(U\hat{u}-\frac{\mu'\hat{w}}{Re}+\hat{p}\right)\right]+r_0=0, \tag{12b}$$

$$\alpha^2\left(\frac{\mu\hat{v}}{Re}\right)+\alpha(\mathrm{i}U\hat{v})+\theta_0=0, \tag{12c}$$

$$\alpha^2\left(\frac{\mu\hat{w}}{Re}\right)+\alpha\left\{\mathrm{i}\left[U\hat{w}-\frac{(\hat{u}'\mathcal{F}_{UU}+\hat{v}'\mathcal{F}_{UV})}{Re}\right]\right\}+z_0=0, \tag{12d}$$

where

$$r_0=\hat{u}\mathcal{H}_U+\left(\frac{W-\mu'-\mathcal{F}'_{UU}}{Re}\right)\hat{u}'-\frac{2(V+1)\hat{v}}{Re}+U'\hat{w}-\frac{\hat{u}''(\mu+\mathcal{F}_{UU})+(\hat{v}'\mathcal{F}_{UV})'}{Re},$$

$$\theta_0=\hat{v}\mathcal{H}_U+\left(\frac{W-\mu'-\mathcal{F}'_{VV}}{Re}\right)\hat{v}'+\frac{2(V+1)\hat{u}}{Re}+\left(V'-\frac{\mathrm{i}\beta\mu'}{Re}\right)\hat{w}+\mathrm{i}\beta\hat{p}-\frac{\hat{v}''(\mu+\mathcal{F}_{VV})+(\hat{u}'\mathcal{F}_{UV})'}{Re},$$

$$z_0=\hat{w}\mathcal{H}_{W'}+\left(\frac{W-2\mu'}{Re}\right)\hat{w}'-\frac{\mathrm{i}\beta(\hat{u}'\mathcal{F}_{UV}+\hat{v}'\mathcal{F}_{VV})}{Re}+\hat{p}'-\frac{\mu\hat{w}''}{Re},$$

and

$$\mathcal{F}_{RS}=\tilde{\mu}Re'S',$$

$$\mathcal{H}_T=\left[\mathrm{i}\beta V+\frac{T}{Re}+\frac{\beta^2\mu}{Re}\right].$$

Here, the radial wavenumber α is the eigenvalue. The orientation angle of the stationary vortices with respect to a circle centred on the axis of rotation and the mode number (i.e.,number of spiral vortices on the disk surface) are given, respectively, as

$$\phi=\tan^{-1}\left(\frac{\bar{\beta}}{\bar{\alpha}}\right)\Leftrightarrow\tan\left(\frac{\pi}{2}-\phi\right)=\frac{\alpha r}{\beta}, \tag{13}$$

$$\bar{n}=\bar{\beta}Re. \tag{14}$$

The perturbation quantities imposed on the steady flow arising from the rough surface are subject to zero boundary conditions at both the disk surface and in the far-field. This ensures that the perturbations are contained within the boundary layer. The choice not to impose partial-slip conditions on the perturbing quantities at $z=0$ is deliberate and is taken to avoid double-counting the surface boundary condition at this position; this is consistent with [7, 9, 22]. In any event, the qualitative effect of imposing these conditions on the perturbations has been found to be negligible in all situations. The perturbation Eq. 12 are subject to

$$\hat{u}(z=0)=\hat{v}(z=0)=\hat{w}(z=0)=\hat{p}(z=0)=\hat{w}'(z=0)=0 \tag{15a}$$

$$\hat{u}\left(z\to z_\infty\right)=\hat{v}\left(z\to z_\infty\right)=\hat{w}\left(z\to z_\infty\right)=0 \tag{15b}$$

2.3. Energy Analysis

Following various studies in the literature [23, 7, 8], an integral energy equation for disturbances within the Carreau model is now derived to analyse the underlying physical mechanisms behind the effects of surface roughness. The derivation of the governing energy equations begins by multiplying the linearised momentum Eq. 11 by the disturbance quantities u, v and w, respectively. The sum of the resulting expressions leads to the kinetic-energy equation for the disturbances,

$$
\begin{aligned}
-\Delta_1 K = {} & (uU' + vV')w + \frac{U(u^2+v^2) + W'w^2}{Re} \\
& + \frac{\partial(up)}{\partial r} + \frac{1}{Re}\frac{\partial(vp)}{\partial\theta} + \frac{\partial(wp)}{\partial z} + \frac{up}{Re} - \frac{\mu}{Re}\left[\frac{\partial}{\partial x_i}(u_j\sigma_{ij}) - \sigma_{ij}\frac{\partial u_j}{\partial x_i}\right] \\
& - \frac{\mu'}{Re}\frac{\partial K}{\partial z} - \frac{\mu'}{Re}\left[\frac{\partial(uw)}{\partial r} + \frac{1}{Re}\frac{\partial(vw)}{\partial\theta} + \frac{\partial(ww)}{\partial z} + \frac{uw}{Re}\right] \\
& - \frac{(\tilde{\mu}U'U')'}{2Re}\frac{\partial u^2}{\partial z} - \frac{(\tilde{\mu}V'V')'}{2Re}\frac{\partial v^2}{\partial z} - \frac{(\tilde{\mu}U'V')'}{Re}\frac{\partial(uv)}{\partial z} \\
& - \frac{(\tilde{\mu}U'U')}{Re}\left[\frac{\partial}{\partial z}\left(u\frac{\partial u}{\partial z}\right) - \left(\frac{\partial u}{\partial z}\right)^2\right] - \frac{(\tilde{\mu}V'V')}{Re}\left[\frac{\partial}{\partial z}\left(v\frac{\partial v}{\partial z}\right) - \left(\frac{\partial v}{\partial z}\right)^2\right] \\
& - \frac{(\tilde{\mu}U'V')}{Re}\left[\frac{\partial}{\partial z}\left(v\frac{\partial u}{\partial z}\right) + \frac{\partial}{\partial z}\left(u\frac{\partial v}{\partial z}\right) - 2\frac{\partial u}{\partial z}\frac{\partial v}{\partial z}\right] \\
& - \frac{\tilde{\mu}U'U'}{Re}\left[\frac{\partial}{\partial z}\left(w\frac{\partial u}{\partial r}\right) - \frac{\partial w}{\partial z}\frac{\partial u}{\partial r}\right] - \frac{\tilde{\mu}U'V'}{Re}\left[\frac{\partial}{\partial z}\left(w\frac{\partial v}{\partial r}\right) - \frac{\partial w}{\partial z}\frac{\partial v}{\partial r}\right] \\
& - \frac{\tilde{\mu}U'V'}{Re}\left[\frac{\partial}{\partial z}\left(w\frac{1}{Re}\frac{\partial u}{\partial\theta}\right) - \frac{\partial w}{\partial z}\frac{1}{Re}\frac{\partial u}{\partial\theta}\right] - \frac{\tilde{\mu}V'V'}{Re}\left[\frac{\partial}{\partial z}\left(w\frac{1}{Re}\frac{\partial v}{\partial\theta}\right) - \frac{\partial w}{\partial z}\frac{1}{Re}\frac{\partial v}{\partial\theta}\right]. \qquad (16)
\end{aligned}
$$

where $K = (1/2)(u^2+v^2+w^2)$ is the disturbances kinetic energy and σ_{ij} are the viscous stress terms due to velocity perturbations,

$$\sigma_{ij} = \frac{1}{Re}\left(\frac{\partial u_i}{\partial x_j} + \frac{\partial u_j}{\partial x_i}\right).$$

The $\mathcal{O}\left(1/Re^2\right)$ terms have been omitted, consistent with the neglect of the $\mathcal{O}\left(1/Re^2\right)$ terms in the linearised perturbation Eq. 11. The perturbations are averaged over a single time period and azimuthal mode and then integrated across the entire boundary layer.

$$
\begin{aligned}
& \int_0^\infty \Bigg[\underbrace{U\frac{\partial\overline{K}}{\partial r}}_{a} + \underbrace{\frac{\partial\left(\overline{up}\right)}{\partial r}}_{b} - \underbrace{-\frac{\mu}{Re}\frac{\partial(u\sigma_{11}+v\sigma_{12}+w\sigma_{13})}{\partial r} - \frac{\mu'}{Re}\frac{\partial(uw)}{\partial r} - \frac{(\tilde{\mu}U'U')}{Re}\frac{\partial(w\sigma_{31})}{\partial r}}_{c} \Bigg] \\
& \underbrace{-\frac{(\tilde{\mu}U'V')}{Re}\frac{\partial(w\sigma_{32})}{\partial r}}_{c}\,\mathrm{d}z = \underbrace{\int_0^\infty\left(-\overline{uw}\frac{\partial U}{\partial z} - \overline{vw}\frac{\partial V}{\partial z} - \frac{1}{Re}\overline{w^2}\frac{\partial W}{\partial z}\right)\mathrm{d}z}_{I} - \underbrace{\int_0^\infty \frac{\mu}{Re}\overline{\sigma_{ij}\frac{\partial u_j}{\partial x_i}}\,\mathrm{d}z}_{\mathrm{II}}\Bigg] \\
& \underbrace{-\int_0^\infty \frac{1}{Re}\overline{up}\,\mathrm{d}z + (\overline{wp})_w}_{\mathrm{III}} - \underbrace{\frac{[\mu(u\sigma_{31}+v\sigma_{32}+w\sigma_{33})]_{\mathrm{w}}}{Re}}_{\mathrm{IV}}
\end{aligned}
$$

$$\underbrace{-\int_0^\infty \frac{\overline{u^2U}}{Re}\,\mathrm{d}z - \int_0^\infty \frac{\overline{v^2U}}{Re}\,\mathrm{d}z - \int_0^\infty \frac{\partial\overline{K}}{\partial z}\frac{W}{Re}\,\mathrm{d}z}_{\mathrm{V}}$$
$$\underbrace{-\int_0^\infty \frac{\mu'(u\sigma_{31}+v\sigma_{32}+w\sigma_{33})}{Re}\,\mathrm{d}z + \int_0^\infty \frac{\mu' uw}{Re^2}\,\mathrm{d}z - \frac{(\mu' K)_\mathrm{w}}{Re} - \frac{(\mu' w^2)_\mathrm{w}}{Re} - \int_0^\infty \frac{\mu'' K}{Re}\,\mathrm{d}z}_{\mathrm{VI}}$$
$$\underbrace{-\int_0^\infty \frac{\mu'' w^2}{Re}\,\mathrm{d}z + \int_0^\infty \left[\frac{(\tilde{\mu}U'U')'}{2Re}\frac{\partial u^2}{\partial z} - \frac{(\tilde{\mu}V'V')'}{2Re}\frac{\partial v^2}{\partial z} - \frac{(\tilde{\mu}U'V')'}{Re}\frac{\partial(uv)}{\partial z}\right]\mathrm{d}z}_{\mathrm{VI}}.$$
$$\underbrace{+\int_0^\infty \frac{(\tilde{\mu}U'U')}{Re}\left[\frac{\partial(u\sigma_{31})}{\partial z} - \sigma_{31}^2\right] + \int_0^\infty \frac{(\tilde{\mu}V'V')}{Re}\left[\frac{\partial(v\sigma_{32})}{\partial z} - \sigma_{32}^2\right]\mathrm{d}z}_{\mathrm{VI}}.$$
$$\underbrace{+\int_0^\infty \frac{(\tilde{\mu}U'V')}{Re}\left[\frac{\partial(u\sigma_{32}+v\sigma_{31})}{\partial z} - 2\sigma_{31}\sigma_{32}\right]\mathrm{d}z - \int_0^\infty \frac{(\tilde{\mu}U'U')\sigma_{31}}{Re}\frac{\partial w}{\partial r}\,\mathrm{d}z - \int_0^\infty \frac{(\tilde{\mu}U'V')\sigma_{32}}{Re}\frac{\partial w}{\partial r}\,\mathrm{d}z}_{\mathrm{VI}}. \tag{17}$$

Here an overbar denotes a period-averaged quantity, such that $\overline{uv} = uv^* + u^*v$ (where * indicates the complex conjugate), and the subscript W denotes quantities evaluated at the wall. Terms on the left-hand side of Eq. 17 can be identified as: (a) the average disturbance kinetic energy convected by the radial mean flow; (b) work done by the perturbation pressure; and (c) work done by the viscous stresses across the boundary layer. On the right-hand side we have: (I) the Reynolds-stress energy production term; (II) the viscous dissipation energy term; (III) pressure work terms; (IV) contributions from work done on the wall by viscous stresses; (V) terms arising from streamline curvature effects and the three-dimensionality of the mean flow; and (VI) the non-Newtonian viscosity terms. The energy equation is then normalized by the integrated mechanical energy flux to give

$$-2\bar{\alpha}_\mathrm{i} = \underbrace{(P_1+P_2+P_3)}_{I} + \underbrace{D}_{II} + \underbrace{(PW_1+PW_2)}_{III} + \underbrace{(S_1+S_2+S_3)}_{IV}$$
$$+ \underbrace{(G_1+G_2+G_3)}_{V} + \underbrace{(N)}_{VI}. \tag{18}$$

3. Results and discussion

3.1. Mean flow

The steady mean-flow equations Eqs. 5 are solved using shooting method. The resulting profiles are depicted in Figs. 1–3 at three examples of surface roughness for various values of n. We fix the value of k parameter at 100 in order to maintain consistency throughout the remainder of this study; and this is consitent with [19]. Our numerical code for the steady flow

has been validated against various prior studies in the literature. In particular, our numerical values reported in Table 1 agree entirely with [22, 7] when $n = 1$, and with [24] when $n \neq 1$. In all calculations we use the integration domain $0 < z < 20$ up through the boundary layer. We find that this leads to converged far-field values at all n and λ, η, and further increases beyond $z_\infty = 20$ have no material effect on the results. This domain is consistent with related studies in the literature [25, 14, 26].

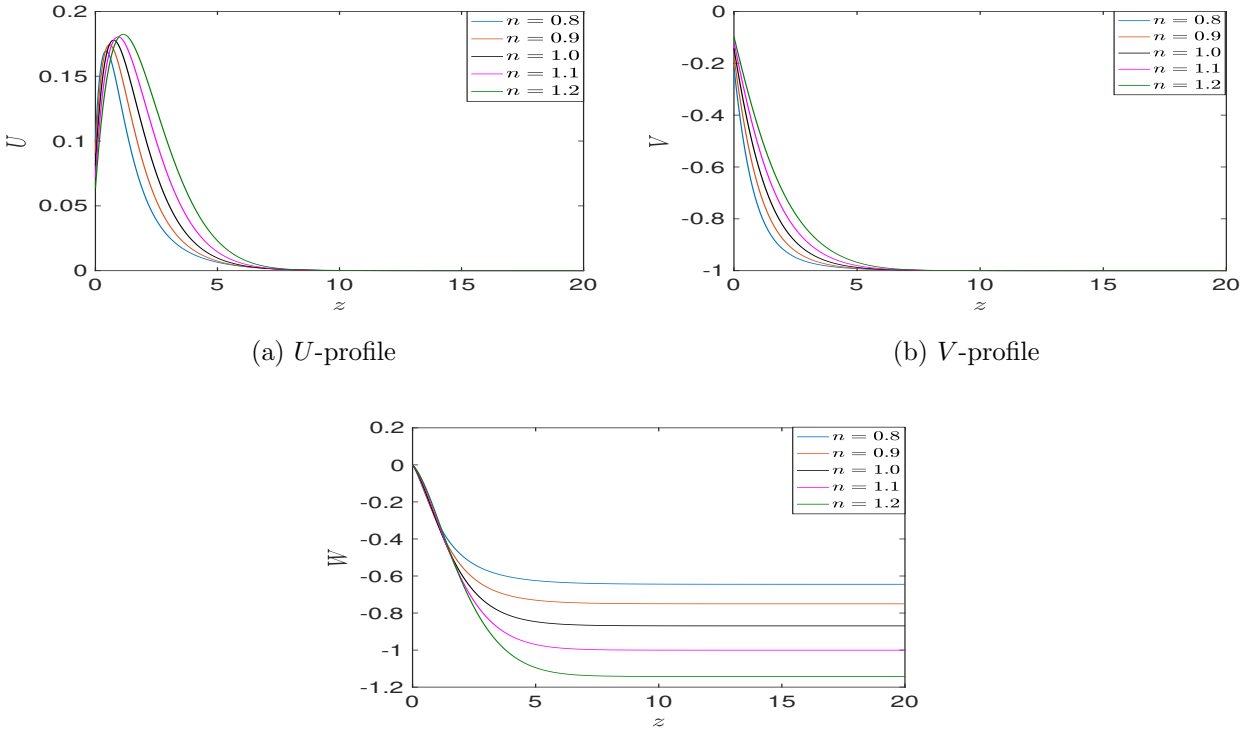

(a) U-profile

(b) V-profile

(c) W-profile

Figure 1: Mean-flow components of the Carreau flow over an isotropically rough disk for shear-thinning and -thickening fluids, $\lambda = \eta = 0.25$.

Fig. 1 shows the mean-flow profiles for isotropic roughness ($\lambda = \eta = 0.25$). The radial-flow profiles reveal that increasing n results in the wall jet moving outwards along the z-axis. That is, the boundary-layer thickness increases with $n > 1$ (shear thickening) and narrows for $n < 1$ (shear thinning). Furthermore, the growth in the peak value shows an increased jet effect for shear-thickening fluids. In the azimuthal velocity profile, the wall value of V increases with n; further evidence of an increasing/narrowing boundary-layer thickness. With regards the normal velocity component, we observe that increasing n leads to greater fluid entrainment into the boundary layer. That is, shear-thickening fluids act to entrain a greater volume of fluid into the boundary layer and shear-thinning a lesser volume. This is consistent with the boundary-layer thickening/thinning effects observed in radial and azimuthal flow components.

Parameters	n	$U'(0)$	$-V'(0)$	$-W(z_\infty)$
Isotropic roughness				
$\eta = \lambda = 0.25$	0.8	0.4016	0.8658	0.6447
	0.9	0.3633	0.7008	0.7503
	1.0	0.4170	0.5034	0.8269
	1.1	0.2873	0.4689	1.0005
	1.2	0.2542	0.3897	1.1424
Radially-anisotropic roughness (concentric grooves)				
$\eta = 0.25$	0.8	0.5904	0.7522	0.6137
	0.9	0.4953	0.6128	0.7134
	1.0	0.4170	0.5034	0.8269
	1.1	0.3534	0.4178	0.9531
	1.2	0.3020	0.3507	1.0906
Azimuthally-anisotropic roughness (radial grooves)				
$\lambda = 0.25$	0.8	0.5736	1.3277	0.7074
	0.9	0.4786	0.9629	0.8190
	1.0	0.4018	0.7251	0.9425
	1.1	0.3401	0.5635	1.0769
	1.2	0.2906	0.4498	1.2211

Table 1: Numerical values of the mean-flow boundary values $U'(0)$, $V'(0)$ and $W(z_\infty)$ for shear-thinning and -thickening fluids, $n = 0.8, 0.9, 1, 1.1, 1.2$, at illustrative values of roughness.

Fig. 2 shows that the effects of increasing the power index for a radially-anisotropic surface roughness ($\eta = 0.25$, $\lambda = 0$) are similar to those in the isotropic case.

Figure Fig. 3 shows the case of radial grooves ($\lambda = 0.25$, $\eta = 0$) and we see mostly similar responses to n in the azimuthal and normal flow components. However, there is some subtly different behaviour observed in the radial profile: while a shear-thickening fluid again acts to thicken the boundary layer, the radial jet is in fact accelerated for *shear-thinning* fluids.

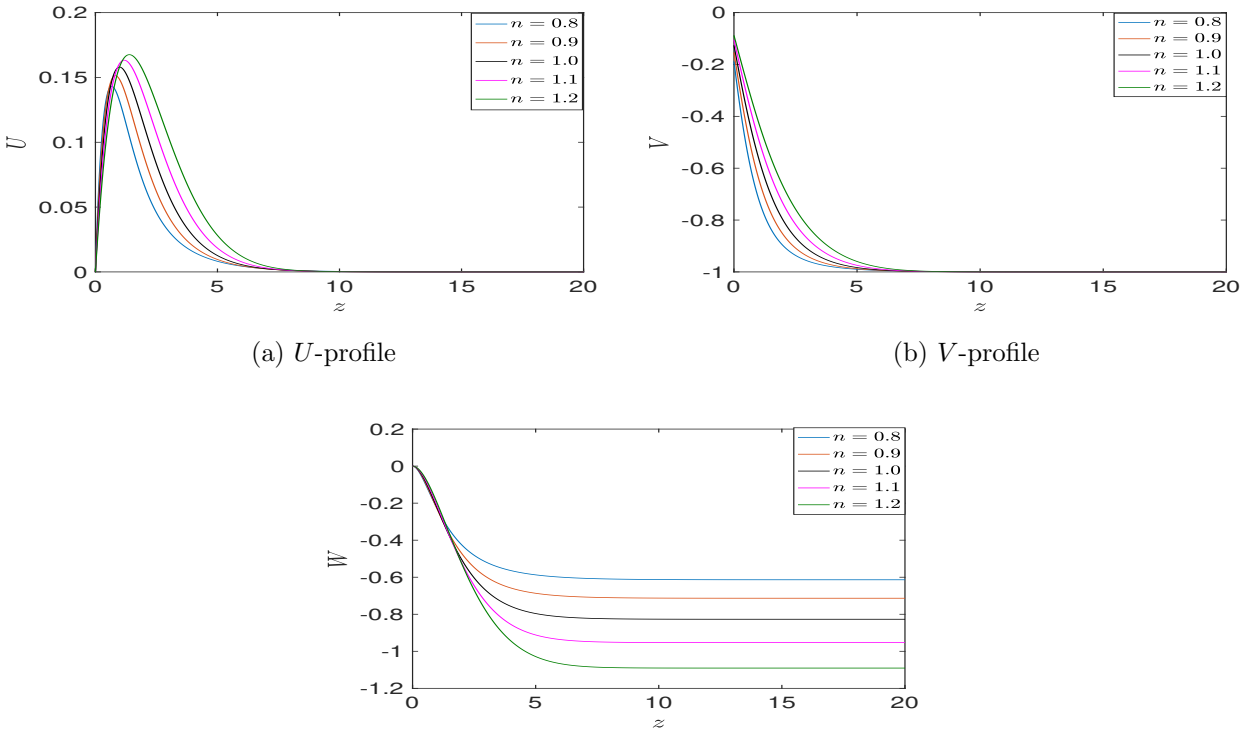

(a) U-profile

(b) V-profile

(c) W-profile

Figure 2: Mean-flow components of the Carreau flow over a radially-anisotropically rough disk for shear-thinning and -thickening fluids, $\eta = 0.25$, $\lambda = 0$.

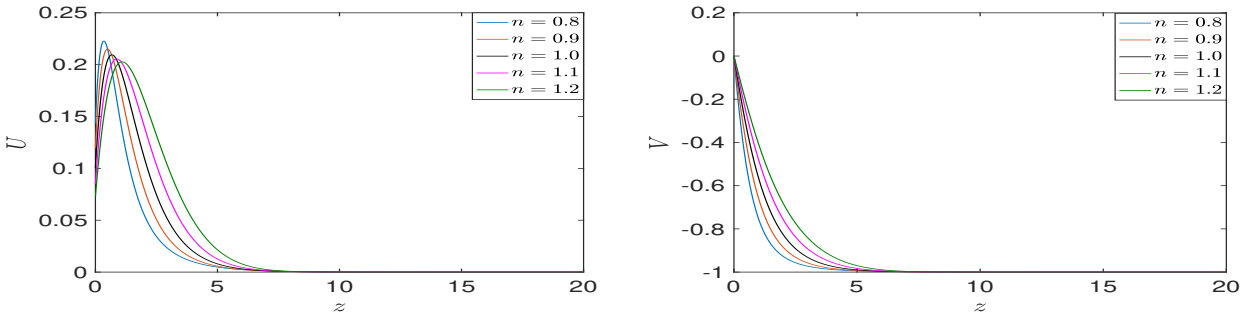

(a) U-profile

(b) V-profile

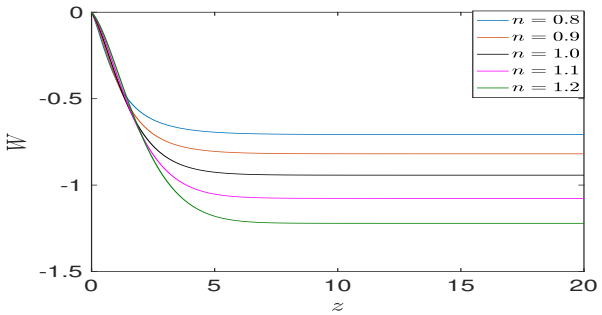

(c) W-profile

Figure 3: Mean-flow components of the Carreau flow over a radially-anisotropically rough disk for shear-thinning and -thickening fluids, $\eta = 0.25$, $\lambda = 0$.

3.2. Convective stability

The eigenvalue problem defined by Eqs. 12 and 15 is solved by implementing a Galerkin projection method based on the collocation approach in terms of the Chebyshev polynomials. All calculations use a Gauss–Lobatto grid with 100 points distributed via an exponential map for the domain between the lower disk surface $z = 0$ and the top of the domain $z = z_\infty = 20$. Further increases in the resolution and spatial extent of this grid were found to have negligible numerical effect on the results of the stability analysis. For further details of this method, the interested reader is referred to Alveroglu et al. [10]. We are concerned with stationary

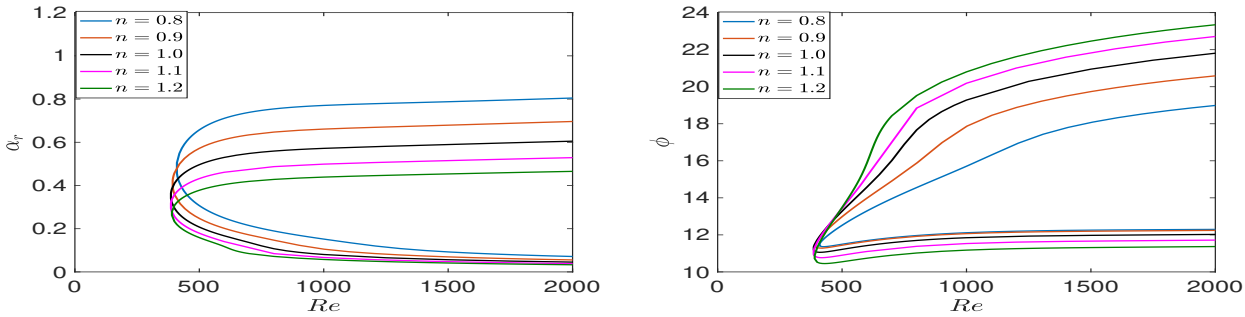

(a) Isotropic roughness

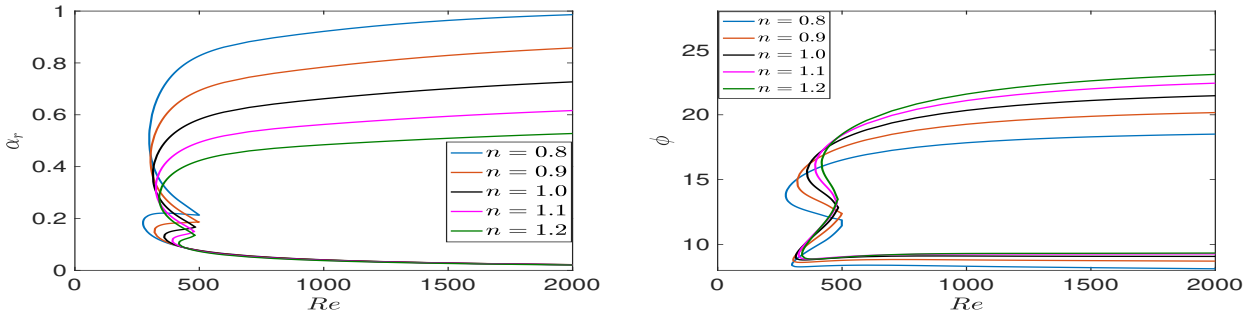

(c) Radially-anisotropic

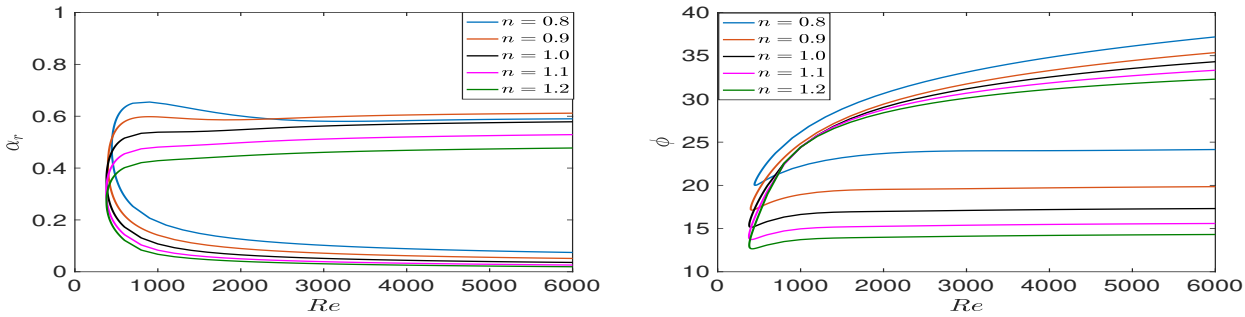

(e) Azimuthally-anisotropic

Figure 4: Neutral curves and the angle for the convective instability for $n = 0.8$, 0.9, 1.0, 1.1, 1.2 with $\eta = 0.25$, $\lambda = 0$.

vortices that rotate with the rough surface and so set $\omega = 0$ throughout the analysis. We

proceed to investigate the structure of the spatial branches by solving the dispersion relation $D(\alpha, \beta; Re, \lambda, \eta, k, n) = 0$ for α whilst marching through values of β at fixed Re.

For all n in the particular range of interest, two spatial branches are found to determine the convective instability characteristics of the system. Neutral curves, defined by neutral spatial growth $\alpha_i = 0$, have been calculated for a variety of shear-thinning and -thickening fluids using the Carreau viscosity model with the rough surfaces. The Type I mode results from the (inviscid) inflectional behaviour of mean-flow components and appears as the upper lobe in neutral curves. The Type II mode arises from the (viscous) streamline curvature and Coriolis effects and appears as a smaller lower lobe. Example neutral curves resulting from our analyses are shown in Figs. 4 and critical Reynolds numbers for the onset of instabilities are shown in Table 2.

Figs. 4 show that stability of the boundary layers over isotropic and azimuthally-anisotropic rough surfaces is dominated by the Type I mode; this is evident from their single-lobed structure. The data presented in Table 2 further suggests that further movement in n either side of this acts to stabilise the boundary layer in terms of increasing the critical Reynolds number. However, it is clear that shear-thinning fluids have the greatest stabilising effect.

In contrast, both Type I and II modes are important over radially-anisotropic rough surfaces, as shown by the distinct lobes in Fig. 5. Furthermore, we see that shear-thinning fluids are *de-stabilising* over such surfaces and the critical Reynolds numbers of both modes are increased with increased n. Although our results are only presented for $\lambda, \eta = 0.25$, similar qualitative behaviour is obtained at all other roughness levels. They do, however, show a substantial decrease in the vortex angle ϕ along both the upper and lower branches of the neutral curves with increased roughness; this is alongside the strong stabilising effect on the Type I mode.

It is also important to consider the influence of roughness on the neutral curves for shear-thinning and thickening Carreau fluids respectively. As shown in Figs. 5 (a), (b), (e) and (f), increasing the levels of isotropic and azimuthally-anisotropic roughness has strong stabilising effects on both the Type I and Type II instability modes of both shear-thinning and thickening flows. On the other hand, one can see from Figs. 5 (c) and (d) that the effect of increasing anisotropic roughness in a concentrically grooved disk is to diminish the Type I lobe whilst destabilising the Type II mode.

The growth rates of the Type I instability mode are presented for shear-thinning and -thickening Carreau fluids for the three cases of the roughness at $Re = Re_c + 25$; that is, at a fixed distance into the neutral curve. Note that the growth rate of the instability mode is measured as the absolute value of the negative imaginary part of the radial wavenumber,

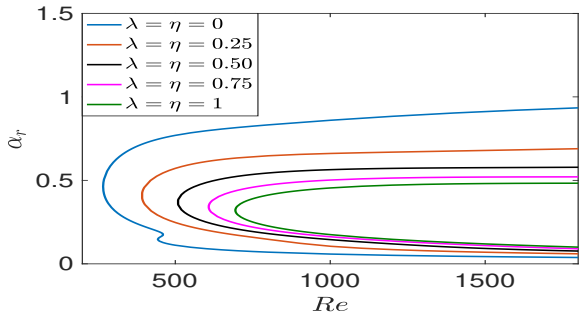

(a) Isotropic roughness with n = 0.9.

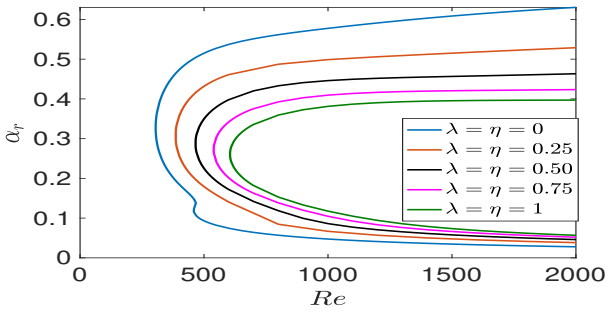

(b) Isotropic roughness with n = 1.1.

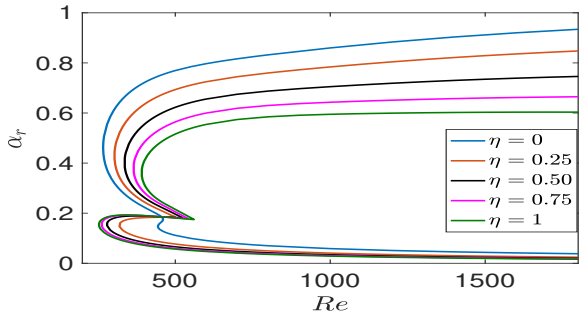

(c) Radially-anisotropic with n = 0.9.

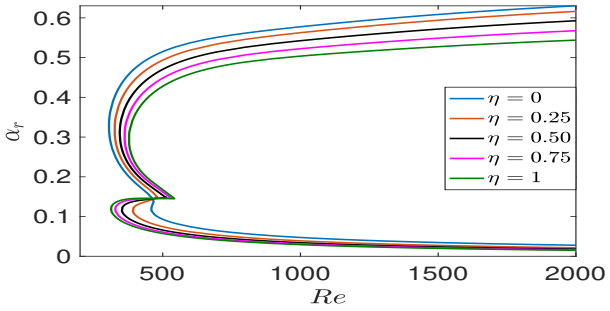

(d) Radially-anisotropic with n = 1.1.

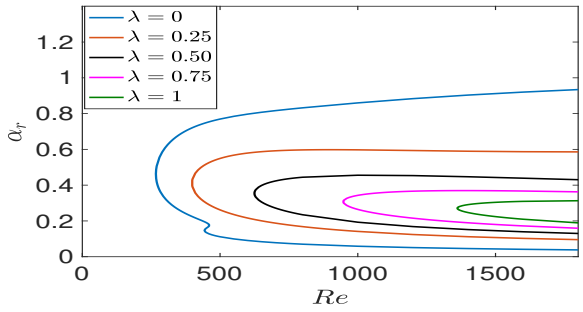

(e) Azimuthally-anisotropic with n = 0.9.

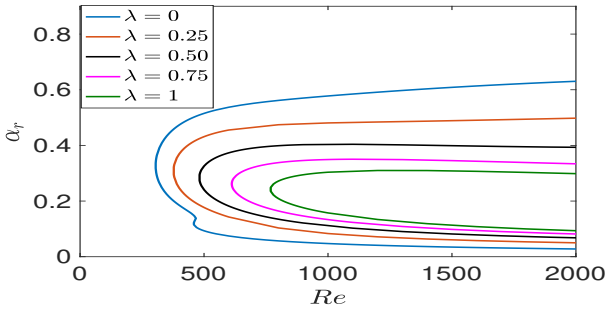

(f) Azimuthally-anisotropic with n = 1.1.

Figure 5: Neutral curves for the convective instability for shear-thinning and thickening with the three cases of roughness with $\eta = 0.25$, $\lambda = 0$.

$|\alpha_i|$, at particular values of the mode number $\bar{n}$. The Type II mode vanishes at even modest levels of all surface roughness under our model and so is not considered here. Fig. 6(a) and (c) reveal the stabilising effect on the growth rates of the Type I mode for both isotropic and azimuthally-anisotropic roughness. That is, even though there appears to be some stabilising effect in terms of the onset of instability (Re_c) when moving n either side of $n = 1.1$, the subsequent development of that instability is quelled only by shear-thinning fluids. In contrast, Fig. 6(b) shows shear-thickening fluids to be the most stable in terms of the delayed onset of instability and the weakest subsequent development for radially-anisotropic surface roughness. It is also interesting to note the effect that shear-thinning and -thickening fluids have on the mode number (number of spiral vortices) $\bar{n}$ under all roughness types: the number of spiral vortices is reduced with increased n.

Parameters	n	Re	$\bar{n}$	ϕ
Isotropic roughness				
$\lambda = \eta = 0.25$	0.8	408.49(−)	39.81(−)	12.11(−)
	0.9	392.20(−)	32.44(−)	12.24(−)
	1.0	385.36(−)	27.04(−)	12.11(−)
	1.1	385.11(−)	22.98(−)	11.71(−)
	1.2	389.45(−)	20.12(−)	11.36(−)
Radially-anisotropic roughness (concentric grooves)				
$\eta = 0.25$	0.8	298.51(273.67)	22.54(12.32)	8.11(13.77)
	0.9	303.65(319.19)	20.21(12.81)	8.71(14.79)
	1.0	313.09(358.72)	18.35(13.03)	9.07(15.60)
	1.1	323.12(391.33)	16.76(12.97)	9.26(15.94)
	1.2	338.80(417.76)	15.45(12.74)	9.33(16.21)
Azimuthally-anisotropic roughness (radial grooves)				
$\lambda = 0.25$	0.8	444.46(−)	78.18(−)	24.15(−)
	0.9	398.21(−)	51.18(−)	19.84(−)
	1.0	380.68(−)	37.31(−)	17.31(−)
	1.1	377.04(−)	29.23(−)	15.58(−)
	1.2	380.86(−)	24.03(−)	14.31(−)

Table 2: The values of the critical Reynolds number Re, $\bar{n}$ and wave angle ϕ on the both modes type I and (type II).

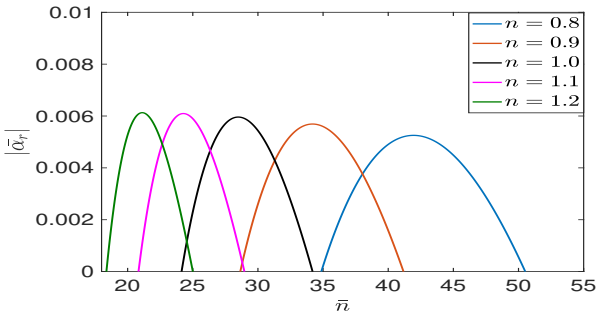

(a) Isotropic roughness

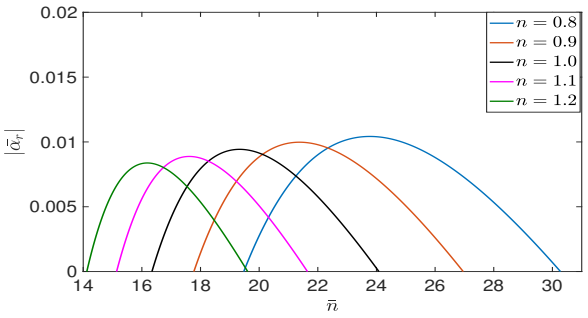

(b) Radially-anisotropic

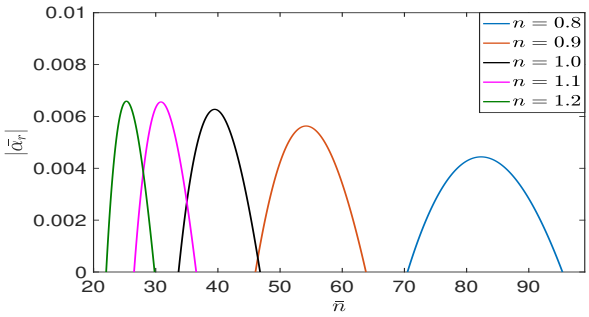

(c) Azimuthally-anisotropic

Figure 6: Growth rates of Type I instability at $Re = Re_c + 25$ for $n = 0.8, 0.9, 1.0, 1.1, 1.2$ for $\eta = 0.25$, $\lambda = 0$.

3.3. Energy analysis Results

The energy balance calculation is carried out at the location of maximum amplifications of the both Type I mode at $Re = Re_c + 25$. Here Re_c is the critical Reynolds number for the onset of the Type I mode of instability for the particular rough surface being considered. Results for various levels of roughness are compared to Newtonian case in Fig. 7.

Fig. 7 (a) demonstrates the energy balance calculation for isotropic roughness. Clearly a stabilization effect obtained in the Type I mode due to a strong decrease in total energy of the flow as n parameter is increased. The main reason of this effect is the large reductions in the energy production term $P2$ and the energy dissipation term D . The changes in the other terms seem to be negligible. Fig. 7 (b) shows a similar stabilizing effect of radially-anisotropic roughness on the Type I mode.

In contrast to isotropic and radially-anisotropic cases, Fig. 7(c) indicates a destabilization effect on the Type I mode in case of azimuthally-anisotropic roughness. In particular, increased power index n leads to growth in the energy production term P_2.

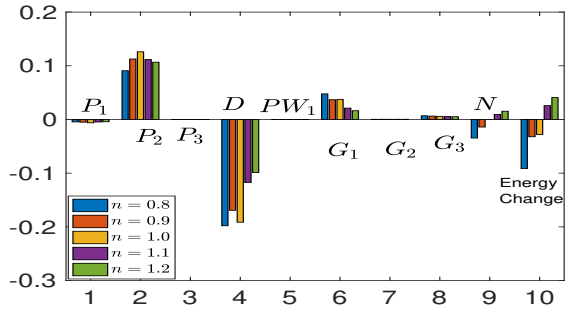

(a) Isotropic roughness

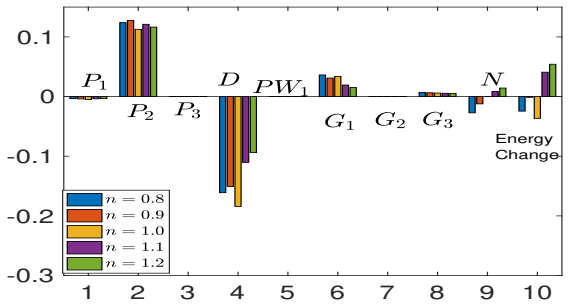

(b) Radially-anisotropic

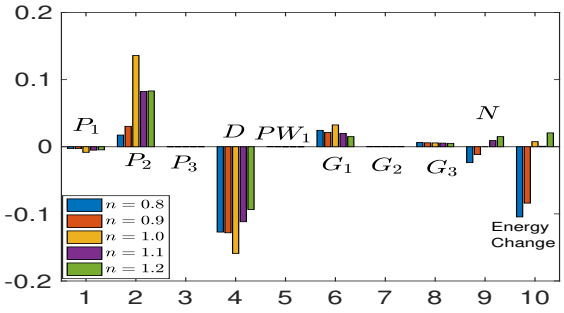

(c) Azimuthally-anisotropic

Figure 7: Energy balance of Type I instability at $Re = Re_c + 25$ for $n = 0.8$, 0.9, 1.0, 1.1, 1.2 for $\eta = 0.25$, $\lambda = 0$.

4. Conclusion

We have studied the convective instability of the boundary-layer flow over rough rotating disks for a category of non-Newtonian fluids abiding by the generalised viscosity law due to Carreau. The main focus has been to examine the effects on the stability of this flow over rough surfaces. To this end, partial-slip boundary conditions have been applied under the MW approach to model a rotating disk with isotropic, radially- and azimuthally-anisotropic surface roughness. The problem has been formulated in a rotating reference frame attached to the disk; all disturbances are assumed to be stationary in this frame.

Mean-flow profiles have been obtained for a range of shear-thinning and -thickening flows over the three surface conditions A subsequent linear stability analysis is then performed on each that solves the radial-wave-number eigenvalue problem with a collocation approach based on Chebychev polynomials. Neutral curves have been calculated that prescribe the parameter regions for instability and critical values of the Reynolds number, spiral vortex number and spiral vortex orientation angles have been computed. Furthermore, the growth rates of the dominant instability mode have been considered a fixed distance into the neutral curve and a complimentary energy analysis completed.

Similar to the von Kármán Newtonian boundary-layer flow over smooth surfaces, the non-Newtonian flow over rough surfaces exhibits two types of instability: the Type I mode originating inviscid effects, and the Type II mode viscous effects. It is found that the introduction of surface roughness has an obvious stabilising effect on both shear-thinning and -thickening flows in general. Each of the three types of surface roughness considered here postpone the onset of the Type I instability by increasing the critical Reynolds number, and both isotropic and azimuthally-anisotropic surface roughness eliminates entirely the Type II mode instability. This is consistent with the results of Cooper et al. [7], Alveroglu et al. [10] for Newtonian flows.

The response of the instability modes to changing the shear-thinning and -thickening properties of the fluid is more subtle. For both isotropic and azimuthally-anisotropic surface roughness, there appears to be a particular value of $n > 1$ (that is, shear-thickening fluid) that gives the minimum critical Reynolds number. Any changes to n either side of this lead to delayed instability, with particular sensitivity observed for shear-thinning fluids. The maximum growth rates within the unstable regime are found to reduce linearly with increasingly shear-thinning fluids. In contrast, shear-thickening fluids are more stable for radially-anisotropic roughness, in-terms of both the delayed onset of instability and its subsequent linear growth.

Our study has revealed that radially-anisotropic roughness (concentric grooves) and isotropic roughness acts to reduce energy production of the Type I mode. Conversely, azimuthally-anisotropic roughness (radial grooves) is found to have the opposite destabilization effect on the Type I mode. The results of this study show that a carefully designed surface roughness with the effect of n parameter led to a stabilization in the flows that can be encountered in many engineering applications.

In view of the results of the current theoretical study, it will be instructive to conduct relevant experiments in future research to verify the analysis presented here. Of additional interest would be an investigation of the non-parallel effects for Carreau flows using the approaches developed by, for example, Davies and Carpenter [27].

Refrences

[1] T. von Kármán, Über laminare und turbulente Reibung, Z. Angew. Math. Mech. 1 (1921) 233–252.

[2] N. Gregory, J. T. Stuart, W. S. Walker, On the stability of three-dimensional boundary layers with applications to the flow due to a rotating disk, Phil. Trans. R. Soc. Lond. A 248 (1955) 155–199.

[3] M. R. Malik, The neutral curve for stationary disturbances in rotating-disk flow, J. Fluid Mech. 164 (1986) 275–287.

[4] P. Hall, An asymptotic investigation of the stationary modes of instability of the boundary layer on a rotating disc, Proc. R. Soc. Lond. A 406 (1986) 93–106.

[5] M. Miklavčič, C. Wang, The flow due to a rough rotating disk, Zeitschrift für angewandte Mathematik und Physik ZAMP 55 (2) (2004) 235–246.

[6] M. S. Yoon, J. M. Hyun, J. S. Park, Flow and heat transfer over a rotating disk with surface roughness, International journal of heat and fluid flow 28 (2) (2007) 262–267.

[7] A. J. Cooper, J. H. Harris, S. J. Garrett, M. Özkan, P. J. Thomas, The effect of anisotropic and isotropic roughness on the convective stability of the rotating disk boundary layer, Phys. Fluids 27 (2015) 014107.

[8] S. J. Garrett, A. J. Cooper, J. H. Harris, M. Özkan, A. Segalini, P. J. Thomas, On the stability of von Kármán rotating-disk boundary layers with radial anisotropic surface roughness, Phys. Fluids 28 (2016) 014104.

[9] S. O. Stephen, Effects of Partial Slip on Rotating-Disc Boundary-Layer Flows, in: 8th AIAA Theoretical Fluid Mechanics Conference, Denver, 2017.

[10] B. Alveroglu, A. Segalini, S. J. Garrett, The effect of surface roughness on the convective instability of the BEK family of boundary-layer flows, Euro. J. Mech. (B/Fluids) 56 (2016) 178–187.

[11] B. Alveroglu, A. Segalini, S. J. Garrett, An energy analysis of convective instabilities of the Bödewadt and Ekman boundary layers over rough surfaces, European Journal of Mechanics-B/Fluids 61 (2017) 310–315.

[12] R. B. Bird, R. C. Armstrong, O. Hassager, Dynamics of polymeric liquids. Vol. 1: Fluid mechanics, Wiley, 1987.

[13] P. Mitschka, J. Ulbrecht, Nicht-Newtonsche Flüssigkeiten IV. Strömung Nicht-Newtonsche Flüssigkeiten Ostwald-de Waelescher Typs in der Umgebung Rotierender Drehkegel und S chieben, Coll. Czech. Chem. Comm. 30 (1965) 2511–2526.

[14] P. T. Griffiths, Flow of a generalised Newtonian fluid due to a rotating disk, J. Non-Newtonian Fluid Mech. 221 (2015) 9–17.

[15] P. T. Griffiths, S. O. Stephen, A. P. Bassom, S. J. Garrett, Stability of the boundary layer on a rotating disk for power law fluids, J. Non-Newtonian Fluid Mech. 207 (2014) 1–6.

[16] P. T. Griffiths, S. J. Garrett, S. O. Stephen, The neutral curve for stationary disturbances in rotating disk flow for power-law fluids, J. Non-Newtonian Fluid Mech. 213 (2014) 73–81.

[17] E. C. Bingham, An investigation of the laws of plastic flow, Bull. U. S. Bur. of Standards 13 (1916) 309–352.

[18] P. J. Carreau, Rheological Equations from Molecular Network Theories, Trans. Soc. Rheolo. 16:1 (1972) 99–127.

[19] P. T. Griffiths, Hydrodynamic stability of non-Newtonian rotating boundary-layer flows, Ph.D. thesis, University of Birmingham, 2016.

[20] P. Griffiths, Stability of the shear-thinning boundary-layer flow over a flat inclined plate, Proc. R. Soc. A 473 (2205) (2017) 20170350.

[21] C. Navier, Mémoire sur les lois du mouvement des fluides, Mémoires de l'Académie Royale des Sciences de l'Institut de France 6 (1823) (1823) 389–440.

[22] B. Alveroğlu, The convective instability of the BEK system of rotating boundary-layer flows over rough disks, Ph.D. thesis, University of Leicester, 2016.

[23] A. J. Cooper, P. W. Carpenter, The stability of rotating-disc boundary-layer flow over a compliant wall. Part 1. Type I and II instabilities, J. Fluid Mech. 350 (1997) 231–259.

[24] M. A. Abdulameer, The Convective Instability of BEK Family of Non-Newtonian Rotating Boundary-Layer Flows, Ph.D. thesis, University of Leicester, 2018.

[25] S. Garrett, N. Peake, The stability of the boundary layer on a sphere rotating in a uniform axial flow, European Journal of Mechanics-B/Fluids 23 (2) (2004) 241–253.

[26] M. Abdulameer, P. Griffiths, B. Alveroğlu, S. J. Garrett, On the stability of the BEK family of rotating boundary-layer flows for power-law fluids, Journal of Non-Newtonian Fluid Mechanics 236 (2016) 63–72.

[27] C. Davies, P. W. Carpenter, Global behaviour corresponding to the absolute instability of the rotating-disc boundary layer, Journal of Fluid Mechanics 486 (2003) 287–329.